Microporous and Mesoporous Materials 139 (2011) 179–188

Contents lists available at ScienceDirect

Microporous and Mesoporous Materials

journal homepage: www.elsevier.com/locate/micromeso

EPR study of the adsorption of dioxin vapours onto microporous carbons and mesoporous silica

M. Francesca Ottaviani [a,*], Roberto Mazzeo [b], Nicholas J. Turro [c], Xuegong Lei [c]

[a] Department of Geological Sciences, Chemical and Environmental Technologies, University of Urbino, Loc. Crocicchia, 61029 Urbino, Italy
[b] Department of Man, Environment and Nature Sciences, University of Urbino, 61029 Urbino, Italy
[c] Department of Chemistry, Columbia University, New York, NY 10027, USA

ARTICLE INFO

Article history:
Received 6 August 2010
Received in revised form 25 October 2010
Accepted 26 October 2010
Available online 31 October 2010

Keywords:
EPR
AC
MTS
Surface characterization
Dioxin

ABSTRACT

Computer aided analysis of electron paramagnetic resonance (EPR) spectra of tetrachloro-dibenzodioxin labelled with a nitroxide radical (TCDD-T) was employed to investigate the adsorption of dioxin vapours onto two carbons, the activated carbon (AC) NORIT GL50 and a carbon directly taken from a waste incinerator (WI) plant, termed EVN.2, and a low-polar micelle-templated mesoporous silica, termed lpMTS. Several experimental conditions were varied to optimize the adsorption process and to mimic dioxin adsorption occurring in a WI plant. Solvent vapours did not perturb dioxin adsorption. EPR analysis suggested that the nitroxide labelled-dioxin interacted (dipole–dipole interactions) with oxygenated groups, mainly C–O–C groups of the carbon and siloxane groups of lpMTS. The kinetics of adsorption was analyzed at different flow rates. The adsorption was large for NORIT and lpMTS already after few seconds, but a complete adsorption was achieved with a slow kinetics, whereas the EVN.2 sample showed a negligible adsorption even after 1 min. The results are interpreted in terms of the surface characterization (S_{BET}, pore volume and pore size distribution) of the adsorbents. The EPR method described in this study can provide useful and unique information on the adsorption process of dioxins onto microporous carbons and mesoporous MTSs. Moreover, this method may be applied to different adsorbates and porous adsorbents.

1. Introduction

Activated carbons (ACs) are widely used as adsorbents and separation media [1–5]. The ACs adsorb different molecular species and an extensive literature describes adsorption of a various assortment of organic molecules, mainly aromatic [2–5]. The adsorption by ACs becomes quantitative for oxygenated planar molecules like dioxins. An AC is expected to efficiently adsorb dioxins due to the high specific surface area (between 300 and more than 1000 m^2/g). The micro- and meso-porosities contain oxygen sites, such as ether, hydroxyl and carboxylic groups that bind the oxygen groups of these pollutants. However, the specific interactions occurring between dioxins and AC surface have not been clarified in the literature.

In the present study, we selected two ACs to investigate their adsorption ability towards dioxin vapours. The first one is the commercially available NORIT GL50 (simply termed NORIT), the second one was directly taken from a waste incinerator (WI) plant and it is termed EVN.2. This latter carbon is inspected on skills to completely adsorb dioxins from flue gas. Indeed, the EC admitted amount of tetrachloro-dibenzodioxin (TCDD) in the emission gas from an incinerator plant is as low as 0.1 ng/N m^3. Therefore it is of paramount importance to study the dioxin-adsorption process of a carbon or another adsorbent directly used in a WI plant, and it is of great interest to well understand the adsorption process of dioxin at the adsorbent surface.

Recently, we have synthesized and characterized the adsorption capability of a particular mesoporous micelle templated silica (MTS) obtained by using a trimethylbenzene (TMB)/cethyltrimetilamonium bromure (CTAB) = 13 (molar-ratio) ratio mixture as templating agent [6,7]. This TMB/CTAB ratio showed to produce a low polar (lp) silica surface and mesoporosities of about 8 nm diameter. We henceforth call this material as lpMTS. The characterization of the adsorption capability indicated a very good affinity for molecules of size and polarity similar to TCDD [7]. Therefore, in the present study, lpMTS was used for TCDD adsorption to be compared to NORIT and EVN.2 adsorption results.

To follow and characterize the adsorption of dioxin onto lpMTS, NORIT and EVN.2 surfaces we employed the electron paramagnetic resonance (EPR) technique by labelling TCDD and dibenzodioxin

* Corresponding author. Address: University of Urbino, Department of Geological Sciences, Chemical and Environmental Technologies (DiGeoTeCA), Scientific Campus Sogesta – Loc. Crocicchia, 61029 Urbino, Italy. Tel.: +39 0722 304320; fax: +39 0722 304240.
E-mail address: maria.ottaviani@uniurb.it (M.F. Ottaviani).

1387-1811/$ - see front matter © 2010 Elsevier Inc. All rights reserved.
doi:10.1016/j.micromeso.2010.10.040

(DD) with a nitroxide probe. Henceforth in this study these spin-labelled dioxins are termed TCDD-T and DD-T, respectively. Since preliminary results demonstrated that the two dioxins were equivalent in respect of their adsorption onto lpMTS, NORIT and EVN.2, we only describe the results obtained with TCDD-T. The TCDD-T interactions with the solid surface were investigated by computer analysis of the EPR spectra obtained after adsorption and discussed in terms of the surface characterization of the solids obtained by nitrogen sorption isotherms at 77 K.

We have previously analyzed adsorption of paramagnetic species onto MTS and carbon surfaces from solution by means of EPR and surface characterization [7,8]. However, it proved to be a challenge to analyze adsorption of the labelled dioxin from the vapour phase, and to reasonably reproduce the adsorption conditions occurring in a WI plant. Usually, in a WI plant [9–13], the gas formed after waste-material burning goes in contact for few seconds with AC powder injected into the gas flow. As an alternative, a fixed AC bed may be used. In any case, an almost quantitative removal (<0.1 ng TEQ/N m^3) of dioxin from the flue gas is needed at this stage.

Therefore, to try to reproduce the WI plant conditions for dioxin adsorption onto lpMTS, NORIT and EVN.2, it is necessary to control a large number of variables such as gas pressure, pollutant concentration, eventual co-adsorbents and their relative amounts, temperature and the effective solid surface/volume coming in contact with the gas phase. We propose a method which makes use of the temperature controlling equipment, available for warming/cooling samples inserted into the EPR cavity, which allowed us to produce a temperature- and pressure-controlled flow of TCDD-T vapour from solutions in different solvents directly into the EPR cavity. Therefore TCDD-T adsorption was investigated by computer aided analysis of EPR spectra recorded over time. The adsorption mechanism onto porous carbon and MTS surfaces is well known to be a slow process, and the kinetics is strongly dependent on the availability of the adsorption sites (in turn depending on pore size, and, generally, on the solid structure), pressure and temperature [14–16]. The kinetics of adsorption of TCDD-T onto NORIT, EVN.2, and lpMTS was analyzed under different experimental conditions and correlated with surface characterization data such as surface area and pore size distribution.

2. Experimental

2.1. Materials

All the chemicals, unless otherwise specified, were purchased from Sigma–Aldrich.

Reagent grade water was obtained from a Milli-Q water purification system (Millipore, Bedford, MA, USA).

AC Norit GL50 Nederland B.V. (simply termed NORIT) was obtained from the manufacturer. AC EVN.2 was directly taken from a WI plant with the purpose to characterize its adsorption properties.

LpMTS was synthesized and characterized as described in the literature [6,7].

Glass fibres (yarn of E type glass) were a gift from Vetrotex-Saint Gobin, Milan, Italy.

Before using these solid materials in the adsorptions studies, the powders were dried overnight in oven at 110 °C. To obtain reproducible results (from EPR and surface characterization) from EVN.2 samples it was necessary to perform the overnight drying procedure in a vacuum oven in presence of acidic water vapours.

2.2. DD-T and TCDD-T synthesis

DD- and TCDD-carboxylic acid were first prepared by following the literature method [17], with some modifications as follows. DD or TCDD (10.8 mmol) and *N*,*N*,*N*′,*N*′-tetramethylethylenenediamine (11.9 mmol) in 40 cm^3 of THF were cooled to −30 °C; 4.6 cm^3 2.5 M (11.5 mmol) of *n*-BuLi was added, stirred for 1 h, then CO_2 was bubbled through, the reactants temperature was raised to room temperature, ether was added and extracted with 2 N NaOH solution. The solution was acidified with diluted hydrochloric acid and extracted with methylene chloride. After chromatographic separation on silica gel, DD-COOH and TCDD-COOH were obtained. The above acids were reacted with 4-hydroxy-2,2,6,6 tetramethyl piperidine N-oxyl, termed Tempol [18] to provide DD-T and TCDD-T. MS (*m*/*z*): 382 (M^+), 366 (M^+-O), 211 (M^+-TEMPO). ^1H NMR (400 MHz, $CDCl_3$, TMS): d 7.48 (s, broad, 1H), 7.05 (d, 1H), 6.98 (s, broad, 3H), 6.9 (d, 2H). The chemical structure of DD-T and TCDD-T are reported in Fig. 1. Since the adsorption results obtained by means of DD-T and TCDD-T were similar to each other, we henceforth only describe those by means of TCDD-T.

2.3. Instrumentation

The EPR spectra were recorded by means of a EMX-Bruker spectrometer operating at X band (9.5 GHz), interfaced to a computer (Bruker software) for data acquisition and handling.

The Bruker ST3000 variable-temperature assembly was used to control both pressure and temperature of the nitrogen flow which carries dioxin vapours to the adsorbent sample into the EPR cavity, as described in the following.

Nitrogen adsorption–desorption experiments were performed at 77 K with a COULTER SA 3100 surface analyzer.

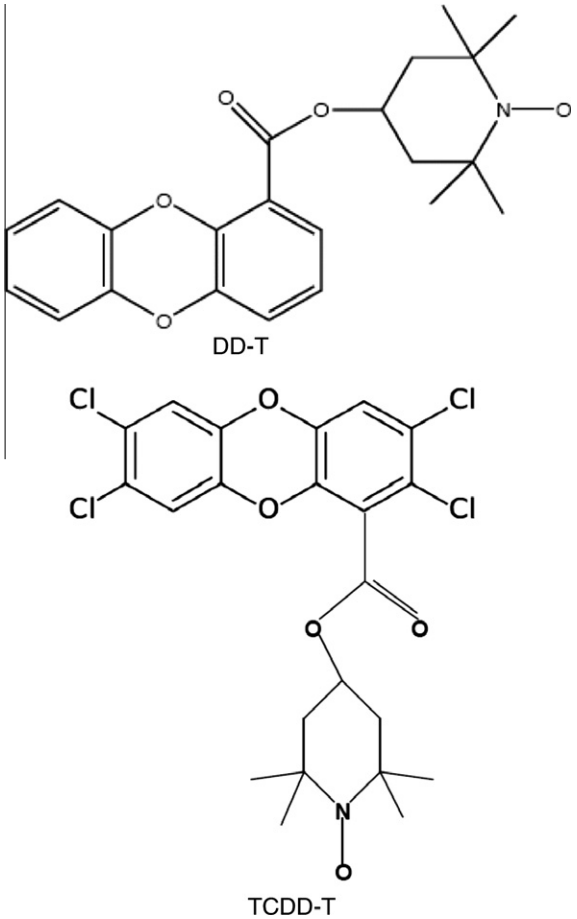

Fig. 1. Chemical formulas of the adsorbates: Tempo-labelled dibenzodioxin (DD-T) and Tempo-labelled tetrachloro-dibenzodioxin (TCDD-T).

2.4. Adsorption apparatus and experimental conditions

Table 1 lists the different experimental conditions and Fig. 2 shows the details of the experimental setup. In summary, a nitrogen flow progressively removes and transports TCDD-T and solvent molecules from a solution to the sample inserted into the EPR cavity. The sample is a homogeneous mixture of the adsorbent (ACs or lpMTS) and glass fibres. These glass fibres were previously tested as unable to adsorb the dioxin and able to create a sponge structure where the flow passes through, favouring the contact between vapour molecules and carbon surface. This system reasonably reproduces the dioxin adsorption conditions in a WI plant.

The reproducibility of the EPR results was tested for a minimum of three repeated measurements for different samples of the same adsorbent.

A preliminary test to demonstrate that the nitrogen flow effectively transports TCDD-T together with the solvent was performed using the lpMTS adsorbent. The resulting EPR spectrum was characteristic of nitroxide-labelled dioxin attached to the silica surface, thus confirming the reliability of the EPR method. We also previously measured the initial "dead time" ($t = 0$ in the adsorption kinetics) needed for the dioxin-containing flow to reach the sample in the cavity. This time depends on the flow rate, but the first spectrum in all kinetics analysis (EPR spectra recorded as a function of time at the different flow rates) was recorded after 5 s, which is the dead time at the lowest flow rate. The flow was stopped 30 s after the complete removal of the solution. We report in the present study about adsorption occurring up to one minute, but we also performed adsorption studies for much longer times (up to 4 h), which are not reported since did not provide further information about the adsorption mechanism.

The vapour exiting from the other end of the EPR tube, after the adsorption, was finally conveyed to a downstream trap containing lpMTS, which quantitatively adsorbed all the residual dioxin eventually present in the exiting flow. This was verified by means of the EPR analysis of the downstream trap at the end of the adsorption process.

The filled EPR tubes were weighed before and after the adsorption process to further quantify the adsorbed amount. The weighing procedure anyway did not provide reproducible data with an accuracy of 5–10%. On the other hand, reproducible adsorption data were obtainable by means of the EPR analysis (accuracy within 2%).

The flow rates are expressed in dm^3/h (or L/h) which are the units of the flow meter employed. The selected nitrogen flow rates were 540, 1080, 1400, and 1620 dm^3/h, which in SI units corresponded to 1.5×10^{-4}, 3×10^{-4}, 3.9×10^{-4}, and 4.5×10^{-4} m^3/s, respectively. We calculated the correspondent pressure (p) by means of the equation which relates p with the flow velocity (v) and the nitrogen density ($\rho = 1.25$ kg/m^3):

$$v^2 = 2p/\rho$$

The flow rate may be written in terms of the velocity (v) and the area section of the tube (A):

$$\text{flow rate} = vA$$

Therefore the pressure was calculated by means of the following equation:

Table 1
Different experimental conditions for analyzing the adsorption of TCDD-T onto NORIT, EVN.2, and lpMTS surfaces (all the solids were previously dried overnight in oven at 110 °C).

Flow rate	540 dm^3/h; 1080 dm^3/h; 1400 dm^3/h; 1620 dm^3/h
Solvent (TCDD-T solution)	Ethyl ether (Teb = 35°C); Chloroform (Teb = 61°C); Toluene (Teb = 110°C)
Concentration (TCDD-T solution)	1×10^{-3} M ; 1×10^{-4} M ; 1×10^{-5} M ; 1×10^{-6} M[a]
Volume (TCDD-T solution)	10 cm^3; 20 cm^3
Temperature	35 °C (all solvents); 60°C ($CHCl_3$ and Toluene); 100 °C (Toluene)
Internal diameter of the EPR tube	2 mm; 4 mm
Glass fibres percentage in the sample	100% (reference); 85%; 75%
From-bubbler-to-sample tube length	50 cm; 70 cm

[a] Minimum concentration to obtain a recordable EPR spectrum.

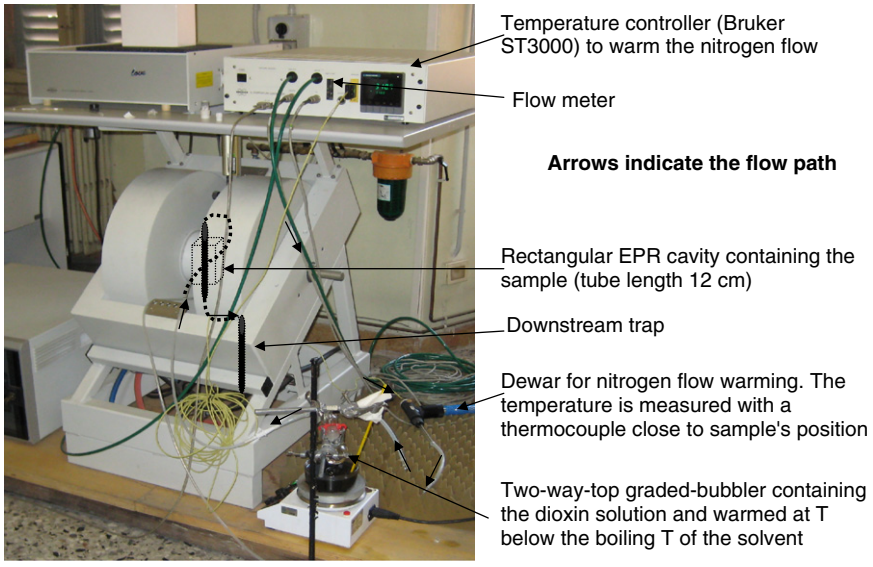

Fig. 2. Scheme of the experimental apparatus for TCDD-T adsorption in the EPR cavity.

$p = [(\text{flow rate})^2 \rho]/(2A^2)$

Considering the radius (1 cm) of the tube exiting the flow-meter, the pressures were calculated from the flow rate values as 0.14, 0.57, 0.96, and 1.28 Pa.

However, the pressure drop from the flow-meter to the EPR cavity cannot be easily quantified, because the flow passes through the bubbler where the solution removal process slows down the flow. Then, the adsorption process in the EPR cavity further and more significantly slows down the flow rate. Since about 7 and 25 s are needed to evaporate 10 cm^3 of solution at 60 °C and at flow rates of 1620 and 540 dm^3/h, respectively, the corresponding flow rates at the bubbler exit are about 5 and 1.45 dm^3/h.

In any case, it is not possible to assess the contact times between TCDD-T and the solid surface based on the initial or the bubbler-exit flow pressures, mainly because of the slow vapour diffusion into the porous solid. This means that a contact time is only quantifiable by analyzing the kinetics of adsorption by EPR.

2.5. Surface characterization

The surface areas and the pore volumes of the solid samples were obtained by means of nitrogen adsorption isotherms at 77 K. The specific surface areas were calculated from the linear parts of the adsorption isotherms (not shown for brevity) using the Brunauer–Emmett–Teller (BET) method [19]. The surface areas and the pore volumes (Table 2) were obtained from Barrett, Joyner, Halenda (BJH) and Broekhof, De Boer (BdB) methods [20,21], the latter being used for mesoporosities. Pore size distribution (Fig. 3) was calculated using density functional theory (DFT) method applied to the nitrogen isotherms.

2.6. Computation of the EPR spectra

Computation of the EPR spectra of the nitroxide in slow motion conditions has been performed by means of the well established procedure by Budil et al. [22]. The main parameter which monitors the interactions of the probes with the surface is the perpendicular component of the correlation time for the rotational motion (τ_{perp}).

Table 2
Total pore volume, and BET areas of the porous solids obtained from nitrogen adsorption/desorption isotherms.

Sample	V_{tot} (cm^3/g)	S_{bet} (m^2/g)
LpMTS	1.67	857
NORIT	0.51	800
EVN.2	5.3	340

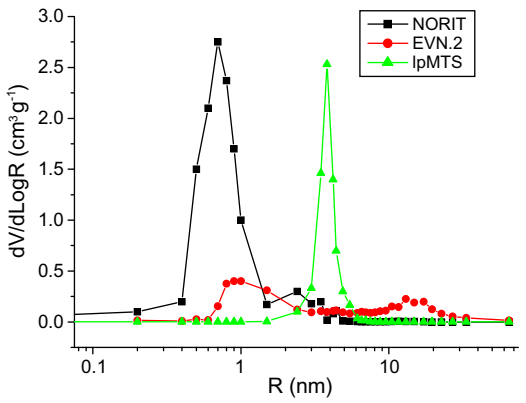

Fig. 3. Pore size distribution of the solids obtained from nitrogen sorption isotherms.

This parameter increases with the decrease in probe mobility, and, therefore, significantly increased when the probes interact and bind to surface groups. The jump rotational diffusional model was used, for which $\tau = 1/D$, where D is the rotational diffusion coefficient. Constant g_{ii} components were assumed (g_{ii} = 2.009, 2.006, and 2.0025) for the coupling between the electron spin and the magnetic field, as already assumed in previous studies for similar systems. The computation provides the main tensor components A_{ii} for the coupling between the electron and the nuclear spins, but we describe the variation of $\langle A_N \rangle = (A_{xx} + A_{yy} + A_{zz})/3$ which changed from one to another system, monitoring the variation in the environmental polarity of the probes.

When the local concentrations of the interacting radicals increase, dipolar spin–spin interactions led to intrinsic line broadening, so, an increase in the line width indicates increased proximity of TCDD-T radicals interacting with close surface sites.

For the carbons, the EPR signal from TCDD-T attached to the carbon surface is superimposed to the signal from paramagnetic centres naturally present in the carbon. By subtracting the spectrum in the absence from that in the presence of attached TCDD-T, we extracted the adsorbed TCDD-T spectral component and then computed it. Subtraction of spectra leads to increase the signal noise. Double integration of the TCDD-T signal provides its intensity value expressed as the adsorbed TCDD-T percentage referred to a 100% of adsorbed TCDD-T. This 100% adsorption was achieved by mixing the solid and the solution and then slowly evaporating the solvent, thus letting TCDD-T completely adsorbed onto the carbon or the lpMTS surface. Spin–spin exchange interactions among condensed paramagnetic species were avoided by a very slow solvent evaporation under stirring: the spectrum was characteristic of adsorbed species, without any line broadening. The adsorbed amount was also calculated as μg of adsorbed TCDD-T/100 mg of adsorbent.

The accuracy of the magnetic (g_{ii}, A_{ii} and $\langle A_N \rangle$) and mobility (τ_{perp}) parameters and of the adsorbed amount (in percentage) extracted from computation is within 2%.

3. Results and discussion

3.1. Reliability of EPR intensity measurements

The first important question to answer before performing the adsorption experiment is about the quantitative relationship between the intensity of the EPR spectrum of TCDD-T in the sample and the effective amount of surface-adsorbed TCDD-T. The literature reports studies dealing on EPR of nitroxides in gas phase [23]. Gas phase spectra of nitroxides are usually not visible due to spin–rotation interaction which largely broadens the spectra. It is known that high pressures increase the collisional relaxation of the rotational angular momentum, thereby narrowing the EPR lines and producing liquid-like EPR signals. So, we could expect that TCDD-T in the nitrogen flow at high pressure would provide a measurable EPR signal. However, we did not see any EPR signal by flowing the TCDD-T vapour in an empty EPR tube inserted in the cavity, probably due to a too rapid flow. On the other hand, we did not detect any EPR signal also by filling the tube with only the glass fibres. Indeed, the glass fibres alone were not able to adsorb the dioxin which went through the sample in the cavity, being completely adsorbed by the downstream lpMTS trap, as shown by the EPR spectrum of the trap at the end of the process (the spectrum is the same as shown in Fig. 4a in other experimental conditions and discussed in Section 3.3). On the other hand, we detected the EPR signal shown in Fig. 4a that increased in intensity over time when the tube was filled with the adsorbents.

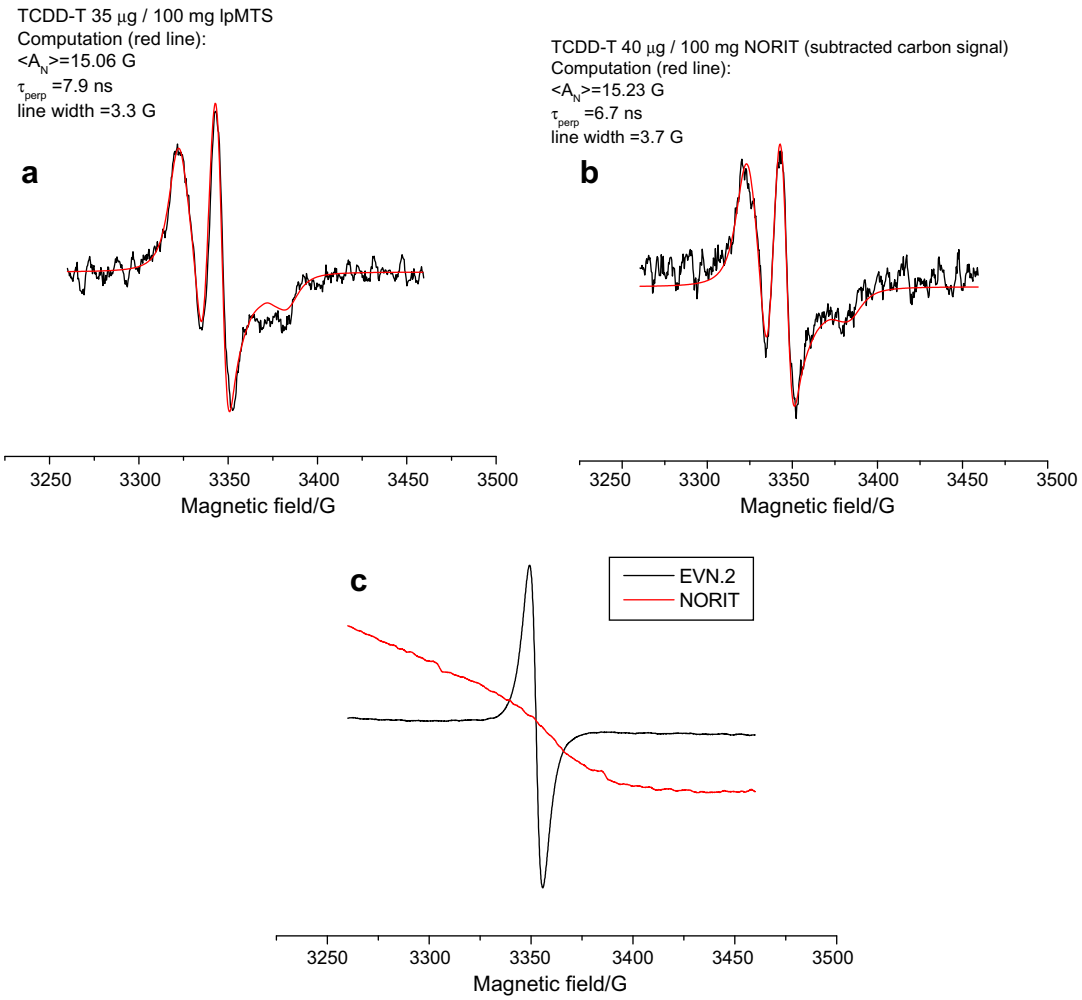

Fig. 4. Experimental (black lines) and computed (red lines) EPR spectra obtained for TCDD-T adsorbed onto lpMTS (a) and NORIT (b). EPR spectra obtained for carbon paramagnetic centres in EVN.2 (black line) and NORIT (red line) before TCDD-T adsorption (c). In case (b) the signal from carbon paramagnetic centres (c) was previously subtracted. The main parameters extracted from computation are also reported. Experimental conditions: $t = 5$ s; 10 cm^3 of TCDD-T solution in $CHCl_3$ at concentration 0.01 mM; T (flow and solution) = 60 °C; N_2 flow rate = 1080 dm^3/h; latex tube length = 50 cm; diameter of the EPR tube = 4 mm; sample mixture constituted by 50 mg of adsorbent and 150 mg of glass fibres. (For interpretation of the references to colour in this figure legend, the reader is referred to the web version of this article.)

The maximum adsorption after 1 min was obtained for lpMTS and corresponded to 97% with respect to the total TCDD-T amount. This high adsorption and the spectral features, characteristic of nitroxides binding the solid surfaces, demonstrated the reliability of the adsorption method described in the present study.

As with all spin labelled molecules, one must consider the effect of the spin label on the process being investigated. So it is important to determine the perturbation generated by the nitroxide "T" group on the adsorption of TCDD. To investigate this issue, the adsorption process was repeated under the same experimental conditions by using either TCDD or TCDD-T. Then, the samples were weighed before and at the end of the adsorption process. The weighing procedure led to a much less accurate analysis than the EPR analysis, that is, the accuracy in the evaluation of the adsorbed amount decreased; but, within the accuracy limit, we found almost the same adsorbed molar amounts of the two species, TCDD and TCDD-T, corresponding to the amounts obtained by means of the EPR analysis and discussed thereafter. Furthermore, the same molar adsorption variations and correspondence with the EPR results were shown for both labelled and unlabelled dioxin by changing experimental variables such as the dioxin concentration and the flow rate. These results indicated that the modality and strength of adsorption are similar for both the species and the nitroxide group does not perturb this adsorption. After validating the equivalence of adsorption of the labelled and unlabelled adsorbents, we may proceed with the analysis of the EPR results.

3.2. Adsorbed TCDD-T percentage on lpMTS in different experimental conditions

Because the main variables affecting TCDD-T adsorption onto the selected adsorbents were the adsorption time and the flow rate, the other experimental conditions listed in Table 1 were first investigated and fixed in order to correctly analyze the adsorption process and its kinetics at the different flow rates. This preliminary check was carried out by means of lpMTS, because in the other cases the subtraction of the carbon signal increased the spectral noise. Table 3 reports the adsorbed percentages of TCDD-T onto lpMTS in different experimental conditions, as obtained from EPR analysis at $t = 5$ s and flow rate = 1080 dm^3/h. The results in Table 3 are summarized and discussed as follows:

– *100% adsorption (reference), and concentration of TCDD-T solution*: first of all it is necessary to emphasize that the same reference, that is, the same total amount of adsorbed TCDD-T was needed for all the experiments in order to correctly compare

Table 3
Adsorbed percentages of TCDD-T onto lpMTS, as obtained from EPR analysis at t = 5 s and flow rate = 1080 dm^3/h; the 100% adsorption reference is obtained by means of TCDD-T totally precipitated from 10 mM of a 0.01 mM solution onto the solid surface, by slowly evaporating the solvent under stirring.

% Fibres	EPR tube size (mm)	TCDD-T concentration (mM)	Solvent	T (°C)	Latex tube length (cm)	%[a] Adsorption
75	2	0.1	Ether	35	50	55
85	2	0.1	Ether	35	50	40
75	4	0.1	Ether	35	50	80–100
75	4	0.01	Ether	35	50	20
75	4	0.01	$CHCl_3$	35	50	17
75	4	0.01	$CHCl_3$	60	50	35
75	4	1	$CHCl_3$	60	50	70
75	4	0.1	$CHCl_3$	60	50	55
75	4	0.001	$CHCl_3$	60	50	15
75	4	0.01	$CHCl_3$	60	70	31
75	4	0.01	Toluene	60	50	30
75	4	0.01	Toluene	100	50	20

[a] Accuracy 2%.

the adsorptions in the different experimental conditions. We selected as 100% reference the total TCDD-T amount deposited from 10 cm^3 of a 0.01 mM solution. In this case, 100% adsorption onto 50 mg of adsorbent corresponded to about 0.1 mg of TCDD-T (molar mass = 520 g/mol) adsorbed onto 100 mg of adsorbent, that is, about 100 μg of TCDD-T for 100 mg of adsorbent. So, the percentage scale corresponds to a μg/100 mg scale. For $CHCl_3$ at 60 °C and flow rates <1620 dm^3/h, the adsorbed percentage linearly increases by increasing TCDD-T concentration (Logarithmic scale). Therefore, the adsorbed percentage was scaled up or down as a function of the concentration at each flow rate.

- *Relative percentage of glass fibres*: a minimum 75% (in weight) of the glass yarn (corresponding to 50 mg of adsorbent and 150 mg of glass fibres) was needed to ensure the passage of the dioxin flow through the sample and to optimize the adsorption. Increasing the glass fibres percentage from 75% to 85% led to a decrease of the adsorption extent because the amount of adsorbent decreases. Furthermore, the too fast flow at 85% did not allow equilibration of the system. Henceforth we used in the adsorption kinetics study only samples with 75% of glass fibres.
- *Volume of the solution*: the adsorption data for the variation of TCDD-T solution volume (from 10 to 20 cm^3) are not reported in Table 3 because the increase in volume simply led to a proportional increase in the adsorbed amount. However, if we use 20 cm^3 instead of 10 cm^3 of solution we need to double time for evaporating all the solution. Therefore we selected a volume of 10 cm^3 for the TCDD-T adsorption studies.
- *TCDD-T solvent*: selecting one or the other of the three solvents (ethyl ether, chloroform and toluene) varied the adsorption extent in line with the different volatility of the solvent. This means that the solvent molecules simply worked as TCDD-T dispersants and carriers and did not compete with TCDD-T for the adsorption sites. Therefore, the solvent, if adsorbed, interacted with different interacting sites with respect to dioxin and did not perturb the adsorption process of TCDD-T. On the basis of the data in Table 3, ethyl ether, due to the low boiling point and consequent easy re-condensation of TCDD-T, gave reproducibility problems when the adsorption extent is very high (between 80% and 100%). On the other hand, toluene showed a decrease in adsorption by increasing temperature from 60 to 100 °C, probably due to (a) simultaneous adsorption/desorption of TCDD-T at 100 °C; (b) degradation of the radical species at high temperature. Conversely, due to a boiling temperature that is in between those of the other two solvents, $CHCl_3$ was well suitable to analyze and compare the kinetics of adsorption of TCDD-T on the different adsorbents at different flow rates.
- *Temperature:* for chloroform solutions, the adsorption increased by increasing T from 35 to 60 °C. Higher temperatures were inconvenient because of a very rapid evaporation of the solution. Therefore, the temperature of 60 °C was selected to perform the TCDD-T adsorption studies.
- *EPR-tube size*: using tubes of 4 mm size asserted accurate and reproducible results of adsorption.
- *Lengths of latex tube from bubbler to EPR tube*: finally, 100% adsorption into the EPR cavity could never be achieved because of TCDD-T loss in the latex tube connecting the bubbler to the EPR cavity (minimum length: 50 cm). On the basis of the adsorption decrease by increasing this length from 50 to 70 cm, we may assume an unavoidable adsorbate loss of 10% into the 50 cm latex tube. However, the higher the flow rate, the lower the adsorbate loss measured. At the highest flow rates, the maximum adsorption obtainable was 97% with respect to the total TCDD-T amount.

3.3. Analysis of the EPR spectra of TCDD-T adsorbed onto the solid surfaces

Fig. 4 shows the experimental and computed EPR spectra obtained for TCDD-T adsorbed onto lpMTS (a) and NORIT (b). The spectra of the carbons before TCDD-T adsorption are also shown (c). The spectra of adsorbed TCDD-T were recorded after 5 s of adsorption and N_2 flow rate of 1080 dm^3/h, and in the optimized experimental conditions described in Section 3.2, that is, by using 10 cm^3 of TCDD-T solution in $CHCl_3$ at a concentration 0.01 mM; with a temperature of the flow and the solutions of 60 °C; with a latex tube of 50 cm length to connect the bubbler to the EPR tube; finally, an EPR tube of 4 mm diameter was filled with a mixture of 50 mg of adsorbent and 150 mg of glass fibres. The spectrum in Fig. 4b was obtained after subtraction of the carbon-alone signal (Fig. 4c) from the carbon plus TCDD-T signal. The main parameters extracted from computation are also reported in the figure.

First, we note that similar spectra were found in the literature for other nitroxide radicals adsorbed from gas phase onto the MTS termed MCM-41 [24]. Furthermore, the same spectral line shapes as those in Fig. 4 were obtained by changing the experimental conditions. The only property which was found to change from one another was the TCDD-T signal intensity due to a variation of the adsorbed amount. Indeed, a line broadening might originate from the highest concentrations at the end of the adsorption process, due to spin–spin interactions between nitroxides adsorbed at proximate sites. Indeed, it is well known that spin–spin interactions occur if the site occupancy is higher than 1 particle every 400 A^2 [24]. In case of lpMTS and NORIT, having a surface area of about 800 m^2/g as measured by BET, the limit of TCDD-T occupancy to avoid spin–spin interactions corresponds to about

3.3×10^{-5} mol/100 mg of adsorbent. This amount is not reached in our adsorption studies even by using the highest TCDD-T concentration of 1 mM (10 cm^3 contain 1×10^{-5} mol). Of course a different situation should occur for EVN.2, since the surface area measured by BET is 340 m^2/g. But, we did not detect a line-broadened signal in this case too, even at the end of the adsorption process and by using the highest TCDD-T concentration, because the adsorbed amount was very low. In the EVN.2 case the TCDD-T signal was at very low intensity even with high TCDD-T concentrations and long adsorption times and therefore the TCDD-T signal came out too noisy after subtracting the carbon signal. Therefore, we could not perform a reliable computation of the signal of TCDD-T adsorbed onto EVN.2. However, it was possible to measure the intensity variation over time, although at the limits of the sensitivity of the EPR technique (as described in Section 3.4).

The EPR signals shown in Fig. 4a and b were characteristic of nitroxide radicals binding oxygen sites at the solid surface and subject to slow motions on the EPR time scale [7]. The computation provides a means for understanding the type and site of interactions that occur between TCDD-T and the surface. From the analysis of the parameters obtained from the computation of the spectra, we extracted the following information:

- First, the environmental polarity of TCDD-T onto NORIT, tested by $\langle A_N \rangle$, was almost the same as found for TCDD-T in ethyl ether solvent ($\langle A_N \rangle$ = 15.2 G; in $CHCl_3$ the polarity is higher because $\langle A_N \rangle$ = 16.1 G). This suggests that the surface interacting sites have the same polarity as ether C–O–C groups, and therefore we propose that C–O–C binding sites are mainly involved in the interactions and binding with dioxin adsorbed on NORIT.
- Interestingly, we note that the polarity is a little bit lower for lpMTS ($\langle A_N \rangle$ = 15.0 G) than for NORIT. This is in line with the higher electron-donor ability of C–O–C groups with respect to Si–O–Si groups [28]. The siloxane site is therefore proposed to be the main binding site of TCDD-T adsorbed at lpMTS surface.
- The strength of the binding interaction, as revealed by τ_{perp}, mainly indicated dipole–dipole interactions. The correlation time is somewhat higher in lpMTS (τ_{perp} = 7.9 ns) with respect to NORIT (τ_{perp} = 6.7 ns). This is explained by geometrical factors, since the lpMTS interacting sites are homogeneously distributed but well spaced on the surface. As a result, the adsorbed probe molecules do not disturb with each other. The hydrogen bonding silanol groups may also play a role in the interactions by anchoring TCDD-T at the lpMTS surface. For NORIT, the strength of interaction is weaker than for lpMTS; probably NORIT microporous structure does not allow TCDD-T to reorganize and orient for optimizing the interactions.
- The better distribution of the interacting sites for lpMTS with respect to NORIT is also consistent with the lower line width for the former (3.3 G) with respect to the latter (3.7 G), since the line width is a measure of the proximity of the radicals.

The different signals recorded from the paramagnetic centres naturally occurring in the two carbons and shown in Fig. 4c also deserve to be discussed. The narrow signal from EVN.2 carbon is characteristic of highly graphitized, poorly activated carbons, whereas the broad signal found for NORIT is characteristic of carbon surfaces containing oxygen sites created by the activation procedure [8,25–27]. From the pore size distribution in Fig. 3, we see that the EVN.2 carbon is very heterogeneous, showing a wide distribution of micro-, meso- and macro-porosities. The EPR characterization tell us further information about EVN.2, such as the presence of graphitized layers and the low capacity to adsorb dioxins.

3.4. Analysis of the adsorption process and its kinetics at different flow rates

Having established the experimental conditions listed in Section 3.2, the adsorption kinetics of TCDD-T were analyzed for the three adsorbents at the four different flow rates.

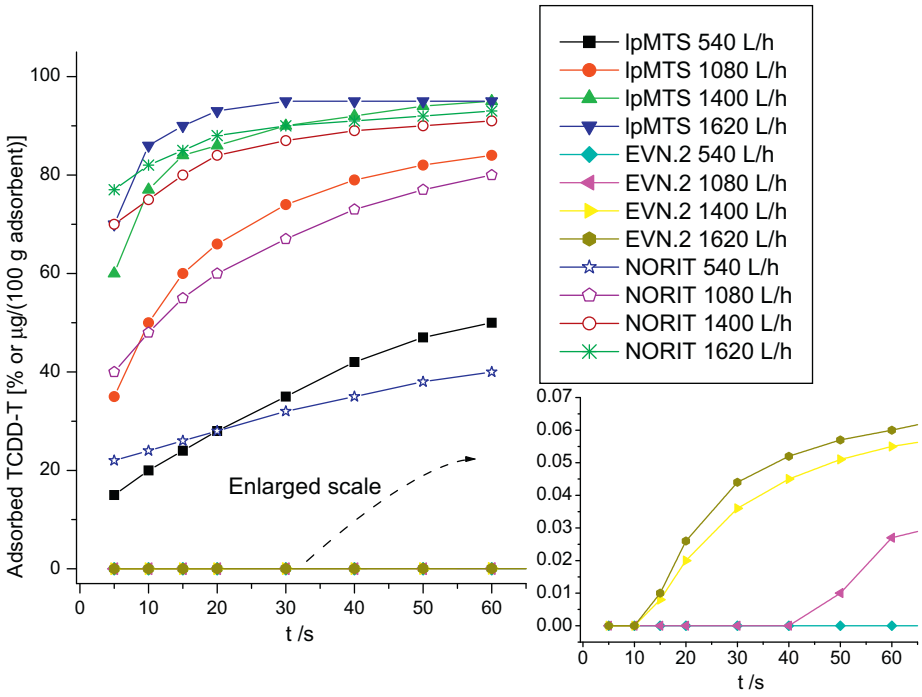

Fig. 5. Kinetics of TCDD-T adsorption on the three adsorbents (lpMTS, NORIT, and EVN.2) at flow rates of 540, 1080, 1400, and 1620 dm^3/h. Selected experimental conditions: 10 cm^3 of $CHCl_3$ solution in the bubbler at concentration of 0.01 mM; 50 mg of adsorbent plus 150 mg of glass fibres; 4 mm diameter EPR tube. In the insert: expanded scale for EVN.2.

The graphs in Fig. 5 show the kinetics of TCDD-T adsorption on the three adsorbents (lpMTS, NORIT, and EVN.2) at flow rates of 540, 1080, 1400, and 1620 dm^3/h. The other experimental conditions were those selected in Section 3.2, and the 100% adsorption corresponded to about 100 μg of adsorbed TCDD-T per 100 mg of adsorbent.

First, we note that the adsorption increases in the sequence EVN.2 ≪ NORIT ⩽ lpMTS. As shown in Fig. 5, an expanded Y scale is required for visualizing TCDD-T adsorption on EVN.2, since EVN.2 adsorption capability results negligible with respect to NORIT and lpMTS. Indeed, after 10 s the adsorption is still 0 for EVN.2 at any flow rate, whereas the adsorption for NORIT and lpMTS at t = 10 s is already significant (from 20% to 90%, depending on the flow rate, as discussed thereafter). This confirms that EVN.2 is not suitable for the use in the WI plant, where the adsorption time is usually very short (about 5 s). This result is in line with the surface characterization data shown in Table 2 and Fig. 3. From these data, the surface available for adsorption for EVN.2 is much lower than the surface of NORIT and lpMTS. However, on the basis of the available surface (Table 2) and the pore size distribution (Fig. 3) we could not expect the total absence of adsorption in the first 10–15 s. To justify this behaviour, we may consider the closing-pore capability of graphitic layers already hypothesized in a previous study on graphitized carbon black [8]: graphitic layers may be able to partially occlude the pore entrance and consequently impede the access of TCDD-T into the pores, where the interacting sites are located. The narrow line in the EPR spectrum of EVN.2 in Fig. 4c is characteristic of the presence of graphitic layers for this carbon which may be considered responsible of micropore occlusion. However, also the presence of negatively charged sites, which repel low polar TCDD-T, and easy desorption occurring in macropores may be responsible of a negligible TCDD-T adsorption. The structure proposed for EVN.2 on the basis of the EPR and surface characterization results is shown in Fig. 6a. Fig. 6 also shows the structures of NORIT (b) and lpMTS (c) and the proposed TCDD-T adsorption sites.

Even if the total adsorbed amount of TCDD-T is higher for lpMTS than for NORIT, the initially quantified adsorption at t = 5 s is higher for NORIT with respect to lpMTS. This may be also rationalized on the basis of the different surface morphology of these two adsorbents depicted in Fig. 6b for NORIT, and c for lpMTS. An initially more effective adsorption on NORIT means that adsorption sites in the microporosities are easily accessible to TCDD-T. This renders this AC well suitable for being used in a WI plant where efficient adsorption must occur in few seconds. Conversely, we found that lpMTS is a better adsorbent than NORIT over time. This suggests that the dioxin-retention capacity of lpMTS is really high. Indeed, we verified that the pollutants remain trapped into the pores even after long times and under high flow rates (results not shown). This is because the channels of lpMTS extend in length and depth (Fig. 6c).

However, a relatively slow kinetics was measured for the remaining TCDD-T. Indeed, the 10 cm^3 of solutions "disappear"

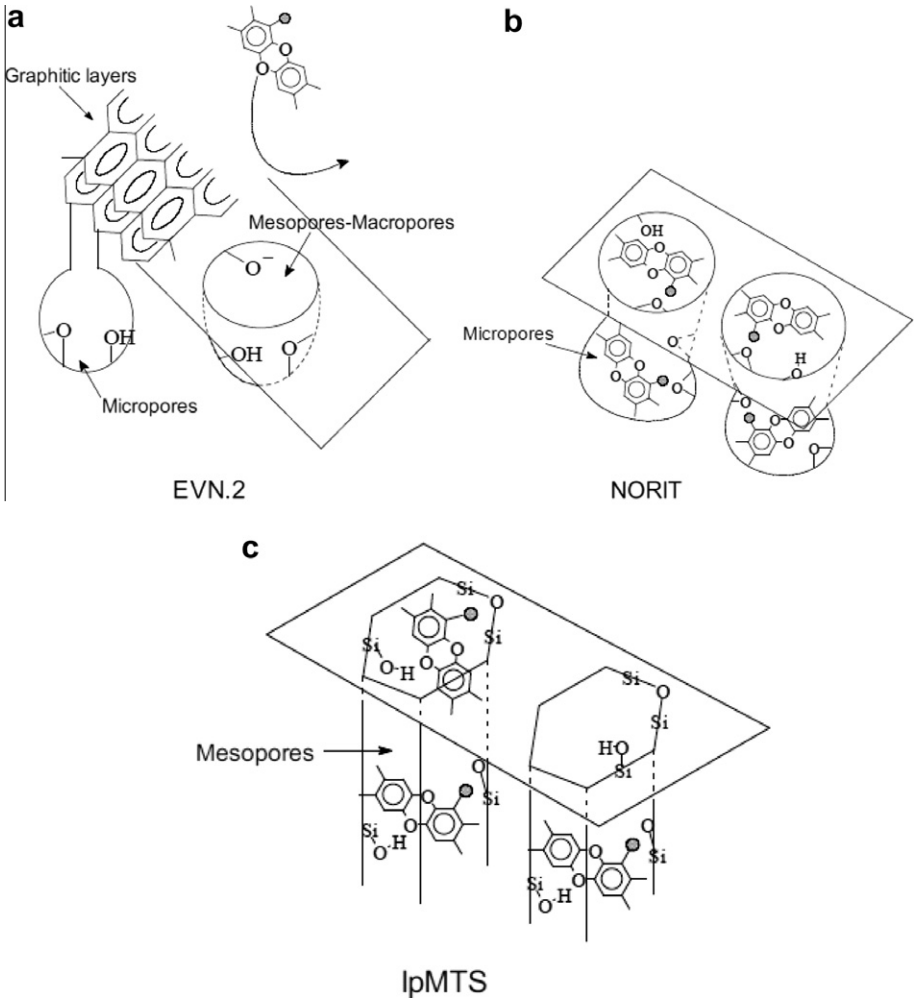

Fig. 6. Proposed structures of the adsorbents and location of TCDD-T: EVN.2 (a); NORIT (b); lpMTS (c).

from the bubbler in a time varying from 25 s at 540 dm^3/h to 7 s at 1620 dm^3/h and the flow was prolonged for 30 s after complete evaporation. So, we expect that the adsorption process would end just after the complete evaporation of the solution, or at least during the flow time, instead in several cases it continues much longer than the flow time. In any case, we see that lpMTS and NORIT almost completely (97%, that is, 97 μg/100 mg) adsorb TCDD-T in the EPR cavity at the end of the adsorption process, but the final time is function of the flow rate (Fig. 5). Therefore, even after complete removal of the solution from the bubbler, some TCDD-T is in the solid sample, but still non-adsorbed, since adsorption continues over time. Slow kinetics of vapour adsorption has been reported for ACs by other authors [14,15], and is due to a slow diffusion rate of vapour into the pores. Diffusion in the pores and channels is obviously impeded by TCDD-T molecules which are initially adsorbed at the pore entrances. When all the easily accessible sites become occupied (after the first seconds), the newly arriving TCDD-T molecules need time for overcoming the barrier created by the already adsorbed ones and displacing them inside the cavities. Consequently, in the porous structures (Fig. 6), a higher flow rate, that is, a higher pressure, facilitates the adsorption, since TCDD-T is strongly forced inside the pores, the barrier is removed, and the kinetics is consequently faster. Interestingly, a faster kinetics was measured for lpMTS with respect to NORIT. This means that the internal porosities of lpMTS were more accessible than those of NORIT. On the basis of the mesoporous hexagonal structure of lpMTS (Fi. 6c), a fast kinetics is well justified, whereas NORIT shows a lower accessibility (a slower occupancy time) of the internal sites, probably due to the more heterogeneous size distribution of channels and pores (Figs. 3 and 6b). However a plateau of adsorption was obtained in some cases even after several minutes (results not reported).

It is evident from the graphs in Fig. 5 that the faster the flow, the greater the adsorption is measured. The main effects of the increasing flow rate are:

(i) increasing amount of TCDD-T transported by the nitrogen flow to the solid surface;
(ii) increasing occupancy of channels and internal porosities where the majority of interacting sites are located;
(iii) promoting adsorption/desorption equilibrium.

Point (i) is equivalently valid for all the solids, but each one may differently host increasing TCDD-T amounts, depending on the number and availability of interacting sites, based on the surface characterization and tentatively depicted in Fig. 6. At the beginning of the adsorption process, NORIT better hosts large amounts of TCDD-T than lpMTS. But, at the highest flow rate, adsorption is also related to the effects described at points (ii) and (iii). The high pressure favours the occupancy of the internal cavities, but TCDD-T diffuses better into the hexagonal lpMTS channels with respect to NORIT. From the graphs in Fig. 5, desorption starts equilibrating with adsorption mainly at a flow rate of 1620 dm^3/h, but this desorption is poorly efficient in the extraction of TCDD-T from the porous structure. The main effect of this strong flow is to favour the diffusion process inside the internal porosities. Therefore, in 30 s during which the flow is active after complete evaporation of the solution, this flow is poorly able to extract TCDD-T molecules from NORIT or lpMTS samples, due to the high number of TCDD-T molecules trapped in the sample and binding to the solid surface. So, after 1 min, the initial pressure followed by diffusion led to an almost complete adsorption of all TCDD-T, which bonds strongly with the oxygen sites. This description did not apply to EVN.2, because the limited availability of interacting sites only allowed a low adsorption even at the highest flow rates, with a very slow kinetics. This particularly limited availability of the pores in the EVN.2 structure is well explained not only by the wide distribution of pore sizes (Fig. 3), but also by the closure of the pore entrance due to external graphitic layers (Fig. 6a).

4. Conclusions

The adsorption process of nitroxide-labelled dioxin, TCDD-T, from gas phase onto two carbons, termed NORIT and EVN.2 (used in a WI plant as dioxin adsorbent), and one micelle templated mesoporous silica, termed lpMTS, was investigated by means of computer aided analysis of the EPR spectra. The experimental conditions were modulated to reproduce those occurring in a WI plant for the removal of dioxins from the waste flow.

After verifying that the adsorbed TCDD-T amount was linearly dependent on TCDD-T concentration (in logarithmic scale) and independent on the type of solvent, the adsorption and its kinetics were followed using 10 cm^3 of TCDD-T solutions in chloroform at 60 °C and at a concentration of 0.01 mM which corresponded to 100 μg of totally adsorbed TCDD-T per 100 mg of adsorbent. The parameters extracted from the computation of the EPR spectra of TCDD-T adsorbed onto NORIT and lpMTS surfaces indicated that the dioxin interacted with oxygenated groups of polarity comparable to C–O–C and Si–O–Si groups, respectively.

The initial adsorption was higher for NORIT than for lpMTS, whereas it was absent for EVN.2, up to 10 s, at all flow rates. However, lpMTS was more efficient in adsorbing TCDD-T than NORIT over time. These differences were related to the different porous structures of the adsorbents which result from the surface characterization by means of nitrogen sorption isotherms. Microporous NORIT presents a higher amount of sites available for the interaction already in the first seconds, whereas mesoporous lpMTS has more accessible and well organized internal interacting sites which contain and stabilize a larger amount of adsorbed TCDD-T over time. Therefore NORIT appears to be well suitable to be used in a WI plant. On the contrary, EVN.2 showed a much lower adsorption capacity than expected on the basis of the available porous surface, probably mainly due to overlapping graphitic layers that reduce access to the internal micropores. By increasing the flow rate, the adsorption increased due to increasing amounts of TCDD-T, but also because high pressure forced the TCDD-T molecules into the pores. But, at the highest flow rates the system approaches the adsorption/desorption equilibrium. The proposed adsorption mechanism for the three adsorbents is roughly depicted in Fig. 6.

Definitely, the EPR method described in this study provides useful information on the adsorption ability and details on the adsorption process of dioxins onto different surfaces, in experimental conditions which mimic the adsorption occurring in a WI plant.

A similar approach may be used for analyzing the adsorption of different pollutants onto any adsorbent.

Acknowledgements

The authors thank Dr. Gian Luca Seravalli of Services and Technologies for the Environment S.p.A. (Florence-Italy) for the useful discussions and for the help in characterizing the carbon structure. The authors also thank Prof. Alberto Modelli (University of Bologna, Italy) for the help in the analysis of the results. The author at Columbia University thank the National Science Foundation for its generous support of this research through grant CHE-07 17518.

References

[1] H. Marsh, F. Rodríguez-Reinoso, Activated Carbon, Elsevier, Oxford, 2006.
[2] R.C. Bansal, M. Goyal, Activated Carbon Adsorption, CRC, Taylor&Francis, Boca Raton, FL, 2005.
[3] T.J. Bandosz, Activated Carbon Surfaces in Environmental Remediation, vol. 7, Elsevier, Oxford, 2006.

[4] E.A. Bottani, J.M.D. Tascon, Adsorption by Carbons, Elsevier, Oxford, 2008.
[5] L.R. Radović, Chemistry and Physics of Carbon, vol. 30, CRC, Taylor&Francis, Boca Raton, FL, 2008.
[6] M.F. Ottaviani, A. Moscatelli, D. Desplantier-Giscard, F. Di Renzo, P.J. Kooyman, B. Alonso, A. Galarneau, J. Phys. Chem. B 108 (2004) 12123–12129.
[7] A. Moscatelli, A. Galarneau, F. Di Renzo, M.F. Ottaviani, J. Phys. Chem. B 108 (2004) 18580–18589.
[8] M.F. Ottaviani, G. Retini, M. Cangiotti, F. Mangani, U. Segre, Spectrochim. Acta, Part A 58 (2002) 1129–1141.
[9] B.G. Miller, Emissions Control Strategies for Power Plants. Coal Energy Systems, Elsevier, San Diego, 2005.
[10] P.S. Kulkarni, J.G. Crespo, C.A.M. Afonso, Environ. Int. 34 (2008) 139–153.
[11] G. McKay, Chem. Eng. J. 86 (2002) 343–368.
[12] H.C. Wang, J.F. Hwang, K.H. Chi, M.B. Chang, Chemosphere 67 (2007) S177–S184.
[13] Y.B. Chang, C.Y. Hung, J.H. Chen, C.T. Chang, C.H. Chen, J. Hazard. Mater. 169 (2009) 1436–1443.
[14] W. Rudzinsk, W.A. Steele, G. Zgrablich, Studies in Surface Science and Catalysis. Equilibria and Dynamics of Gas Adsorption on Heterogeneous Solid Surfaces, vol. 104, Elsevier, Amsterdam, 1997.
[15] A.J. Fletcher, Y. Yüzak, K.M. Thomas, Carbon 44 (2006) 989–1004.
[16] B. Lefevre, A. Saugey, J.L. Barrat, L. Bocquet, E. Charlaix, P.F. Gobin, G. Vigier, Coll. Surf. A Physicochem. Eng. Aspects 241 (2004) 265–272.
[17] B.D. Lalmer, M. Boyd, W.A. Denny, J. Org. Chem. 55 (1990) 438–441.
[18] A. Hassner, V. Alexanian, Tetrahedron Lett. 46 (1978) 4475–4478.
[19] S. Brunauer, P.H. Emmett, E. Teller, J. Am. Chem. Soc. 60 (1938) 309–319.
[20] J.H. de Boer, J.C.P. Broekhof, J. Catal. 3 (1967) 8; 9 (1967) 15; 10 (1968) 153; 10 (1968) 368; 10 (1968) 377; 10 (1968) 391.
[21] E.P. Barrett, L.G. Joyner, P.H. Halenda, J. Am. Chem. Soc. 73 (1951) 373–380.
[22] D.E. Budil, S. Lee, S. Saxena, J.H. Freed, J. Magn. Res. A 120 (1996) 155–189.
[23] S.N. Batchelor, Chem. Phys. Lett. 288 (1998) 119–123.
[24] E.L. Straz, D.A. Chernova, A.K. Vorobiev, Mendeleev Commun. 18 (2008) 246–248.
[25] S. Mrozowski, Carbon 26 (1988) 521–529.
[26] D. Campbell, C. Jackson, H. Marsh, W.F.K. Wynne-Jones, Carbon 4 (1966) 159–166.
[27] L.S. Singer, S. Mitchell, Carbon 35 (1997) 599–604.
[28] M.G. Voronkov, A.Y. Deich, J. Struct. Chem. 5 (1964) 482–489.